

Detecting Statistical Interactions from Neural Network Weights

Michael Tsang Dehua Cheng Yan Liu
 {tsangm,dehuache,yanliu.cs}@usc.edu
 University of Southern California

Abstract

Interpreting deep neural networks can enable new applications for predictive modeling where both accuracy and interpretability are required. In this paper, we examine the weights of a deep neural network to interpret the statistical interactions it captures. Our key observation is that any input features that interact with each other must follow strongly weighted paths to a common hidden unit before the final output. We propose a novel framework, which we call Neural Interaction Detector (NID), that identifies meaningful interactions of arbitrary-order without an exhaustive search on an exponential solution space of interaction candidates. Empirical evaluation on both synthetic and real-world data showed the effectiveness of NID, which detects interactions more accurately and efficiently than does the state-of-the-art.

1 Introduction

The interpretability of machine learning models is important due to implications for communicating these models to a variety of practitioners and stakeholders (Varshney & Alemzadeh, 2016). Interpretability is especially important in domains where decisions can have major consequences (Kim, 2015). For example, in a case study on pneumonia risk prediction from Caruana et al. (2015), an interpretable model learned patterns that previously prevented black-box models from being deployed. This is because risks associated with learning unintended health patterns often prevent practitioners from using such models.

Deep neural networks have been recognized as some of the best performing machine learning methods; however, they are notorious for their black-box, uninterpretable nature (Yosinski et al., 2015). While some works have studied direct methods of interpreting neural networks, including estimating feature importance from weight parameters (Garson, 1991), computing output gradients with respect to input features (Hechtlinger, 2016), and visualizing hidden representations (LeCun et al., 2015; Yosinski et al., 2015), these works do not cover the interpretation of statistical interactions captured by neural networks. Such statistical interactions contain structural information on the function approximated by a neural network, knowledge of which can be valuable for understanding how the model makes predictions over all input data (Ribeiro et al., 2016).

A statistical interaction is a non-additive effect between two or more features on a response variable (Sorokina et al., 2008b). For example, in $y = x_1x_2 + x_3$, the *interaction* is between x_1 and x_2 since they are non-additive, and the additive effect of single features (e.g. x_3) is categorized as a *main effect*. From an interpretable machine learning perspective, interaction detection is useful for building predictive models that are both accurate and interpretable (Lou

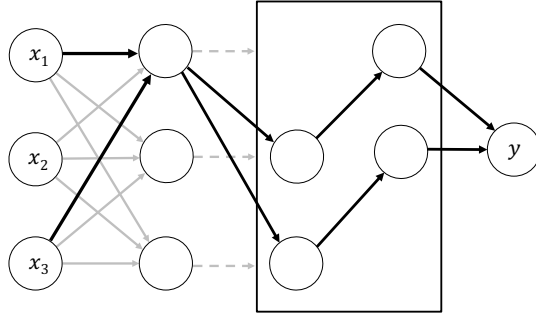


Figure 1: An illustration of an interaction within a fully connected feedforward neural network, where the box contains later layers in the network. The first hidden unit takes inputs from x_1 and x_3 with large weights and creates an interaction between them. The strength of the interaction is determined by both incoming weights and the outgoing paths between a hidden unit and the final output, y .

et al., 2013). From a data analysis perspective, knowledge of interactions allows a domain expert to reason about which individual groups of features affect a response variable in data (Sorokina, 2008a).

In this work, we develop an approach for detecting interactions captured in a neural network by interpreting the neural network parameters. This approach is based on our observation that *any input features interacting with each other must follow strongly weighted connections to a common hidden unit before the final output* (see Figure 1). Provided this structural insight, we have developed a novel and extremely simple algorithm to detect interactions when a deep neural network encodes them. From empirical evidence and theoretical guarantees, our approach contributes an accurate and efficient method for detecting arbitrary-order interactions without searching an exponential solution space of interaction candidates. We achieve these contributions using our framework NID, which generates a shortlist of interactions candidates and ranks them, solely by interpreting the weights of a single trained deep neural network. We show that we can find a cutoff on the ranking to obtain the true interactions by using a special form of the *generalized additive model* (Wood, 2006) that accounts for higher-order interactions.

Our framework presents a new method for detecting statistical interactions and understanding which interactions a neural network captures. Furthermore, the generalized additive model we use to cut off interaction rankings is itself a type of accurate and interpretable model, serving as a novel higher-order extension to GA²Ms (Lou et al., 2013) that are well-acknowledged for their accuracy, interpretability, and editability (Caruana et al., 2015; Ribeiro et al., 2016; Lipton, 2016; Choi et al., 2016; Kim et al., 2016; Varshney & Alemzadeh, 2016; Krause et al., 2016).

Roadmap: We review related works and notations in Section 2. In Section 3, we examine and quantify interactions directly from neural network parameters, which leads to our framework for interaction detection detailed in Section 4. Finally, we demonstrate the practical utility of our framework on both synthetic and real-world data in Section 5.

2 Related Works

Interpretability

A variety of interpretations of deep neural networks can be obtained by *direct* and *indirect* methods. Direct methods examine network parameters or structure to explain predictions, whereas indirect (or posthoc) methods do not utilize such information (Lipton, 2016). There are several techniques for directly interpreting neural networks. For example, Garson (1991) proposed a way estimating feature importance directly from network weight connections, Hechtlinger (2016) found that computing output gradients with respect to input features led to sensible interpretations, and Itti et al. (1998); Mnih et al. (2014); Xu et al. (2015) demonstrated ways of modifying neural architectures to interpret what they focus on for their predictions.

In addition, there are various techniques for indirectly interpreting neural networks. For example, Provost et al. (1997) used sensitivity analysis to analyze feature contributions to a neural network’s output. Ribeiro et al. (2016) developed a technique for probing any black-box model around a prediction of interest to locally explain its decision boundary. Specific to deep neural networks, Che et al. (2015) used a distillation technique to mimic the neural network outputs with a more interpretable model. Several visualization techniques have also been proposed for posthoc neural network interpretability. For example, Maaten & Hinton (2008); LeCun et al. (2015); Mnih et al. (2015) used dimensionality reduction techniques to visualize clusters in hidden representations, and Simonyan et al. (2013); Mahendran & Vedaldi (2015); Yosinski et al. (2015) devised visualization techniques for the output units of convolutional architectures to show human-interpretable images. In contrast to these posthoc approaches, our approach to interpreting statistical interactions in a deep neural network is a direct method.

Few works have found ways to directly interpret the global behavior of a neural network, i.e. how a neural network makes predictions over all data - as opposed to local behavior, i.e. predictions at single data points. Examples of direct interpretations of global behavior are feature importance from network weights, and dimensionality-reduced visualization of hidden representations (Garson, 1991; Maaten & Hinton, 2008; LeCun et al., 2015; Mnih et al., 2015). Our method adds to this list with the introduction of a direct interpretation of statistical interactions captured by a neural network via its weights. In addition, our weight interpretations underwent an empirical and functionally-grounded (Doshi-Velez & Kim, 2017) evaluation, which is oftentimes not possible when evaluating interpretability techniques.

Interaction Detection

The problem of interaction detection is fundamental to statistical analysis (Christensen, 2011). While interactions can be between any number of features, most interaction detection techniques focus on finding *pairwise* interactions rather than higher-order ones because there are less candidates to select from (Fan et al., 2016). Namely, pairwise detection techniques only need to consider p^2 candidates rather than the 2^p candidates needed to find arbitrary-order interactions (where p is the number of input features). There are two ways that leverage the smaller search space of pairwise interaction candidates. One way is to hand-specify each interaction of interest and encode all of such interactions into a single model, where the model is used to isolate true interactions. The other way is to do individual tests for each pairwise interaction and therefore do p^2 individual tests. Early on, Fisher (1925) introduced the concept of Two-way ANOVA, which uses the approach of pre-defining pairwise interactions of interest and encoding all of these terms into a single linear model to conduct significance tests on every interaction. Similarly, Bien et al. (2013) proposed the *hierarchical lasso* framework that encodes all pairwise quadratic interactions into a hierarchical linear model and uses a lasso penalty to identify true

interactions from their coefficient terms. These approaches do not scale well to detecting high order interactions because all 2^p interaction terms would have to be separately encoded into a single model.

There are several approaches for individually testing interaction candidates. Loh (2002) introduced *GUIDE*, which tests each pairwise interaction candidate based on a χ^2 test and constructs a 2×4 contingency table for every tested interaction. Sorokina et al. (2008b) proposed *Additive Groves of Trees (AG)* that tests every interaction candidate by constructing a separate series of regression trees in each test. By testing each and every interaction candidate, these methods need to build separate models for each of the p^2 pairwise interactions, and in the case of *AG*, build 2^p sets of regressions trees to test for all interaction candidates up to the p -th order. In our experiments, we often compare our model to *AG* because *AG* tests for interactions based on exactly their non-additive definition, and *AG* was shown to be capable of high-order interaction detection.

Oftentimes, interaction detection methods require restrictive assumptions on the type of interactions that can be modeled. For example, *ANOVA* and *hierarchical lasso* require pre-selected interaction candidates to be incorporated into their respective models. On the contrary, methods like our approach and *AG* attempt to model interactions of any non-additive form. In particular, the expressive advantage that both our approach and *AG* possess is their ability to fit nonlinear data well. However, since *AG* must construct an exponentially increasing number of models to test higher-order interactions, the chance of obtaining false positives in any test can quickly compound over all tests, leading to a high *false discovery rate*, as known in statistics (Benjamini & Hochberg, 1995). Since we only train a single deep neural network to obtain its ranking of interaction candidates, our method is not susceptible to high false discovery rates that arise from multiple testing.

Notations

Vectors are represented by boldface lowercase letters, such as \mathbf{w} ; matrices are represented by boldface capital letters, such as \mathbf{W} . The i -th entry of a vector \mathbf{w} is denoted by w_i , and element (i, j) of a matrix \mathbf{W} is denoted by $W_{i,j}$. The i -th row and j -th column of \mathbf{W} are denoted by $\mathbf{W}_{i,:}$ and $\mathbf{W}_{:,j}$, respectively. For a vector $\mathbf{w} \in \mathbb{R}^n$, let $\text{diag}(\mathbf{w})$ be a diagonal matrix of size $n \times n$, where $\{\text{diag}(\mathbf{w})\}_{i,i} = w_i$. For a matrix \mathbf{W} , let $|\mathbf{W}|$ be a matrix of the same size where $|\mathbf{W}|_{i,j} = |\mathbf{W}_{i,j}|$.

Let $[p]$ denote the set of integers from 1 to p . An *interaction*, \mathcal{I} , is a subset of all input features $[p]$ with $|\mathcal{I}| \geq 2$. For a vector $\mathbf{w} \in \mathbb{R}^p$ and $\mathcal{I} \subseteq [p]$, let $\mathbf{w}_{\mathcal{I}} \in \mathbb{R}^{|\mathcal{I}|}$ be the vector restricted to the dimensions specified by \mathcal{I} .

Feed-forward Neural Network Consider a feed-forward neural network with L hidden layers. Let p_ℓ be the number of hidden units in the ℓ -th layer, where $p_0 = p$ is the number of input features. There are L weight matrices $\mathbf{W}^{(\ell)} \in \mathbb{R}^{p_\ell \times p_{\ell-1}}$ where $\ell = 1, 2, \dots, L$, and $L + 1$ bias vectors $\mathbf{b}^{(\ell)} \in \mathbb{R}^{p_\ell}$ where $\ell = 0, 1, \dots, L$. Let $f(\cdot)$ be the activation function (non-linearity), and let $\mathbf{w} \in \mathbb{R}^{p_L}$ and $b \in \mathbb{R}$ be the coefficients and bias for the final output. Then, the hidden units $\mathbf{h}^{(\ell)}$ of the neural network and the output y with input $\mathbf{x} \in \mathbb{R}^p$ can be expressed as:

$$\begin{aligned} \mathbf{h}^{(0)} &= \mathbf{x} \\ \mathbf{h}^{(\ell)} &= f\left(\mathbf{W}^{(\ell)}\mathbf{h}^{(\ell-1)} + \mathbf{b}^{(\ell)}\right), \quad \forall \ell = 1, 2, \dots, L \\ y &= \mathbf{w}^\top \mathbf{h}^{(L)} + b. \end{aligned}$$

3 Feature Interactions in Neural Networks

In this section, we identify and quantify influential statistical interactions modeled by a neural network. We often refer to statistical interactions as “feature interactions” when the statistical interactions of interest are between features. By the non-additive definition of a feature interaction and the mathematical formulation of a neural network, all interactions in the neural network are created at hidden units, and their influence is propagated layer-by-layer to the final output, as depicted in Figure 1. We first study and quantify these two stages, then we discuss network architecture considerations to improve interaction detection.

3.1 Interactions at Individual Hidden Units

The notion that feature interactions must be modeled at common hidden units is fundamental to our paper. We prove that this notion is true in Proposition 1. We also argue the reverse statement, that if there are paths being modeled at common hidden units, then features will likely be interacting.

Consider a feedforward neural network as a directed graph where hidden units are vertices and nonzero weights are directed edges pointing to next layers, then we have the following proposition:

Proposition 1 (Interactions at Common Hidden Units). *Let $\varphi(\cdot)$ be a multilayer feedforward neural network. If $\varphi(\cdot)$ contains an interaction \mathcal{I} , then there exists a hidden unit h , such that $\forall i \in \mathcal{I}$, there is a path from i through h to the output in the associated graph. The reverse of this statement is true with probability 1 when the non-zero weights are generated i.i.d. from any continuous distribution.*

We start by proving the first statement. Without loss of generality, we only consider vertices that are connected to the final output. Suppose for the purpose of contradiction that h , as defined in Proposition 1, does not exist. Then for any hidden unit h' in the last hidden layer before the output, we have that $\mathcal{I} \subsetneq \mathcal{S}_{h'}$ where $\mathcal{S}_{h'}$ is the set of all ancestors of h' on the graph. Note that, for any hidden unit h' , it can be viewed as a function $f_{h'}(\mathcal{S}_{h'})$ of all its parents. Then the output $\varphi(\cdot)$ can be rewritten as

$$\varphi = \sum_{h' \text{ in the last hidden layer}} w_{h'} \cdot f_{h'}(\mathcal{S}_{h'}) + b,$$

where $w_{h'}$ is the weight for h' , and b is the bias term for the final output. This is a function without the interaction \mathcal{I} , which is a contradiction.

We provide an argument for the second statement. Note that the second statement is agnostic to the actual distribution of nonzero weights as long as the distribution is continuous, e.g. a uniform distribution on $[-1, 1]$. While it is possible to construct counterexamples to the second statement; that is, examples where there is no interaction between features even if there exists h on a path from i to the output $\forall i \in \mathcal{I}$, any counterexample is subject to fluctuations from randomness in weight distribution. The existence of counterexamples is manifested when early hidden layers capture an interaction that is negated in later layers. For example, the effects of two interactions may be directly removed in the next layer, as in the case of the following expression: $\max\{w_1x_1 + w_2x_2, 0\} - \max\{-w_1x_1 - w_2x_2, 0\} = w_1x_1 + w_2x_2$. Such an counterexample is legitimate; however, the probability of the w_1 s and the w_2 s from the left hand side being exactly equal is zero due to random fluctuations, so such an interaction removal cannot happen in practice.

We have shown that interactions must be captured at common hidden units; however, weights in a neural network are generally nonzero. Therefore, we must provide a measure for which interactions are more important than others. Consider a neural network with a single hidden layer. Any hidden unit in the network can imply up to $2^{\|\mathbf{W}_{j,:}\|_0}$ potential interactions, where $\|\mathbf{W}_{j,:}\|_0$ denotes the number of nonzero values in the weight vector $\mathbf{W}_{j,:}$ for the j -th hidden unit. To determine relative importance of interactions, the notion of an interaction strength must be mathematically defined.

We propose to measure the strength of the interaction with the minimum corresponding weight between interacting features. Namely, for a potential interaction $\mathcal{I} \in [p]$ and the weight vector $\mathbf{W}_{j,:}$ for the j -th hidden unit, the strength of interaction \mathcal{I} , denoted by $\omega(\mathcal{I}, \mathbf{W}_{j,:})$, is defined as:

$$\omega(\mathcal{I}, \mathbf{W}_{j,:}) = \min_{i \in \mathcal{I}} \{|\mathbf{W}_{j,i}|\}.$$

This definition of interaction strength satisfies three key properties:

1. interaction strength is evaluated as zero whenever an interaction does not exist (one of the features has zero weight);
2. interaction strength does not decrease with any increase in magnitude of feature weights;
3. interaction strength is less sensitive to changes in large feature weights.

The first two properties place natural constraints on the behavior of interaction strength. The third property accounts for the sensitivity of interaction strength and is subtle in its intuition. Consider the scaling between the magnitudes of two feature weights, where one weight has much higher magnitude than the other. In the worst case, there is one large weight in magnitude, and the rest of the feature weights are near zero in their magnitudes. If the large weight grows in magnitude, this change may not contribute anything to interaction strength, but if instead the smaller weights grow at the same rate in magnitude, then interaction strength should strictly increase.

To combine feature weights, we considered a representative set averaging methods belonging to the generalized mean family (Bullen et al., 1988): maximum value, root mean square, arithmetic mean, geometric mean, harmonic mean, and minimum value. All of these methods satisfy the second property; however, due to the first property, maximum value, root mean square, and arithmetic mean cannot be used. The remaining methods: minimum value, harmonic mean, and geometric mean all satisfy the third property in addition to the first two. In a thorough empirical evaluation, we found that minimum value yielded the most accurate interaction detection results out of all of the representative averaging methods (see Table 4).

In an example of an simple interaction, we show that we can directly obtain our definition of interaction strength that uses minimum value. Specifically, consider an interaction between two input features x_1 and x_2 in a single-layer neural network with ReLU activation: $\max\{\alpha_1 x_1 + \alpha_2 x_2, 0\}$. We quantify the strength of this interaction by using a simple ReLU approximation that captures the interaction: a quadratic approximation.

Proposition 2. *Let $\beta_0 + \beta_1 x_1 + \beta_2 x_2 + \beta_3 x_1^2 + \beta_4 x_2^2 + \beta_5 x_1 x_2$ be the best quadratic approximation, measured by square loss, to the function $\max\{\alpha_1 x_1 + \alpha_2 x_2, 0\}$ on $(x_1, x_2) \in (-1, 1) \times (-1, 1)$, then for the coefficient of interaction, β_5 , we have that,*

$$\beta_0, \dots, \beta_5 = \underset{\beta_i, i=0, \dots, 5}{\operatorname{argmin}} \iint_{-1}^1 \left[\beta_0 + \beta_1 x_1 + \beta_2 x_2 + \beta_3 x_1^2 + \beta_4 x_2^2 + \beta_5 x_1 x_2 - \max\{\alpha_1 x_1 + \alpha_2 x_2, 0\} \right]^2 dx_1 dx_2.$$

Solving $|\beta_5|$, the magnitude of the coefficient on the quadratic approximation of the $\{x_1, x_2\}$ interaction,

$$|\beta_5| = \frac{3}{4} \left(1 - \frac{\min\{\alpha_1^2, \alpha_2^2\}}{5 \max\{\alpha_1^2, \alpha_2^2\}} \right) \min\{|\alpha_1|, |\alpha_2|\}. \quad (1)$$

Note that the choice of the region $(-1, 1) \times (-1, 1)$ is arbitrary: for larger region $(-c, c) \times (-c, c)$ with $c > 1$, we found that $|\beta_5|$ scales with c^{-1} . By the results of Proposition 2, the strength of the interaction can be well-modeled by the minimum value between $|\alpha_1|$ and $|\alpha_2|$, which satisfies all three desired properties of interaction strength. Note that the factor before $\min\{|\alpha_1|, |\alpha_2|\}$ in Equation (2) is almost a constant with less than 20% fluctuation.

3.2 Measuring the Influence of Hidden Units

Our definition of interaction strength is not complete without accounting for the outgoing paths of those hidden units that capture interactions. For example, if the weights of the outgoing paths of a hidden unit are all 0, then the hidden unit cannot contribute to corresponding interactions. We treat the weights of the outgoing paths as a measure of importance for the hidden unit. In order to formally compute this importance, we draw direct inspiration from Garson’s algorithm (Garson, 1991; Goh, 1995), which computes *feature* importance (rather than hidden unit importance) via cumulative weight matrix multiplications. Intuitively, the importance of a node in a neural network should be measured by its influence on the final output, as contributed by all paths between them. Thus, we define the *aggregated weight* at the i -th hidden unit at the ℓ -th hidden layer as $z_i^{(\ell)}$ to represent the importance of the hidden unit, where $\mathbf{z}^{(\ell)} \in \mathbb{R}^{p_\ell}$ and

$$\mathbf{z}^{(\ell)} = |\mathbf{w}|^\top \left| \mathbf{W}^{(L)} \right| \cdot \left| \mathbf{W}^{(L-1)} \right| \dots \left| \mathbf{W}^{(\ell+1)} \right|,$$

The *aggregated weight* essentially sums over all possible paths from the hidden unit to the final output y .

We show that our definition of *aggregated weight* is a good measure of hidden unit importance by proving it is the Lipschitz constant for corresponding hidden units. The Lipschitz constant in general serves as a global upper bound on the magnitude of the gradient with respect to a variable in question. For example, the Lipschitz constant has been commonly used in importance sampling in stochastic optimization to achieve variance reduction (Needell et al., 2014).

Lemma 3 (Neural Network Lipschitz Estimation). *Let $f(\cdot)$ be a 1-Lipschitz function. Then the output y is $z_i^{(\ell)}$ -Lipschitz with respect to $h_i^{(\ell)}$.*

Proof. For non-differentiable $f(\cdot)$ such as ReLU function, we can replace it with a series of differentiable 1-Lipschitz functions that converges to $f(\cdot)$ in the limit. Therefore, without loss of generality, we assume that $f(\cdot)$ is differentiable with $|\partial_x f(x)| \leq 1$. We can take the partial derivative of the final output with respect to $h_i^{(\ell)}$, the i -th unit at the ℓ -th hidden layer:

$$\begin{aligned} \frac{\partial y}{\partial h_i^{(\ell)}} &= \sum_{j_{\ell+1}, \dots, j_L} \frac{\partial y}{\partial h_{j_L}^{(L)}} \frac{\partial h_{j_L}^{(L)}}{\partial h_{j_{L-1}}^{(L-1)}} \dots \frac{\partial h_{j_{\ell+1}}^{(\ell+1)}}{\partial h_i^{(\ell)}} \\ &= \mathbf{w}^\top \text{diag}(\dot{\mathbf{f}}^{(L)}) \mathbf{W}^{(L)} \dots \text{diag}(\dot{\mathbf{f}}^{(\ell+1)}) \mathbf{W}^{(\ell+1)}, \end{aligned}$$

where $\dot{\mathbf{f}}^{(\ell)} \in \mathbb{R}^{p_\ell}$ is a vector that

$$\dot{f}_k^{(\ell)} = \partial_x f \left(\mathbf{W}_{k,:}^{(\ell)} \mathbf{h}^{(\ell-1)} + b_k^{(\ell)} \right).$$

We can conclude the Lemma by proving the following inequality:

$$\left| \frac{\partial y}{\partial h_i^{(\ell)}} \right| \leq |\mathbf{w}|^\top \left| \mathbf{W}^{(L)} \right| \dots \left| \mathbf{W}_{:,i}^{(\ell+1)} \right| = z_i^{(\ell)}.$$

The left-hand side can be re-written as

$$\sum_{j_{\ell+1}, \dots, j_L} w_{j_L} \dot{f}_{j_L}^{(L)} W_{j_L, j_{L-1}}^{(L)} \dot{f}_{j_{L-1}}^{(L-1)} \dots \dot{f}_{j_{\ell+1}}^{(\ell+1)} W_{j_{\ell+1}, i}^{(\ell+1)}.$$

The right-hand side can be re-written as

$$\sum_{j_{\ell+1}, \dots, j_L} |w_{j_L}| \left| W_{j_L, j_{L-1}}^{(L)} \right| \dots \left| W_{j_{\ell+1}, i}^{(\ell+1)} \right|.$$

We can conclude by noting that $|\partial_x f(x)| \leq 1$. \square

While the absolute values in our aggregated weight definition remove negating effects associated with standard matrix multiplications, these effects are suppressed by a sparsity-inducing regularizer, which we describe in Section 3.4. In addition, in our experiments, we found that not using the absolute values worsens interaction detection performance.

3.3 Quantifying Interaction Strength

As discussed in Sections 3.1 and 3.2, the strength of an interaction has two components: 1) the strength of interaction at a hidden unit, and 2) the influence of hidden units on the final output. For a potential interaction \mathcal{I} and the i -th unit in the first hidden layer $h_i^{(1)}$, the combined interaction strength is $\omega_i(\mathcal{I}) = z_i^{(1)} \omega(\mathcal{I}, \mathbf{W}_{i,:}^{(1)})$. Note that $\omega_i(\mathcal{I})$ is defined on a single hidden unit, and it is agnostic to scaling ambiguity within a ReLU based neural network. In Section 4, we discuss our scheme of aggregating strengths, which is crucial to compare interactions of different orders.

3.4 Architecture and Design Considerations

Sparsity-inducing Penalty In order to filter out spurious interaction candidates, we effectively suppress unimportant interaction paths by imposing sparse-inducing penalties on neural network weights while they train. In our experiments, we find that a sparse penalty boosts the performance of interaction detection.

Many researchers (Goodfellow et al., 2016) have reported that introducing a L1-penalty during training greatly improves the sparsity of the learned network without a noticeable sacrifice on prediction performance. We tune the L1-penalty to maximal network sparsity without major decrease in prediction accuracy on a validation set.

Modeling Main Effect If main effects exist in data and are modeled in a neural network, then their effects can pass through the same hidden units that feature interactions pass through, thus presenting problems for our approach to finding interactions at hidden units. We mitigate

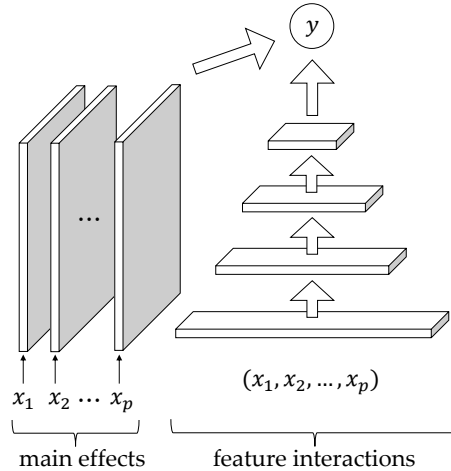


Figure 2: An illustration of the neural network architecture for interaction detection. Main effects are modeled by the lefthand components, which are crucial for minimizing spurious interactions. Features interactions are modeled by the righthand primary neural network.

this problem by adjusting the network architecture to directly model main effects as separate components in the network, as illustrated in Figure 2. In particular, we form an additive model:

$$y = \mathbf{w}^\top \mathbf{h}^{(L)} + b + \sum_{i=1}^p g_i(x_i),$$

where $g_i(\cdot)$ is a nonlinear function of the i -th feature. All $g_i(\cdot)$ are modeled using neural networks, which are trained jointly via backpropagation.

Intuitively, this approach is meant to draw the modeling of main effects away from the interaction component of the neural network (the righthand side of Figure 2). In practice, by modeling main effects as separate components, we found that the interactions we extracted had less false positives.

Sufficient First Hidden Layer As we noted Section 3.3, we use the first hidden layer to propose interactions and their strengths. In order to quantify interaction strengths at hidden units, we rely on there being enough hidden units to extract a sufficient number of interaction candidates that cover true interactions. In practice, we found that as long as there are a sufficient number of hidden units to fit data well, we do not need to purposefully increase the size of the first hidden layer because it is already wide enough for extracting interactions.

Interactions at First versus Intermediate Layers Based on its structure, a deep feed-forward neural network should in theory be able to model interactions at any hidden layer. However, in our experiments we were not able to detect interactions by considering every hidden layer, nor could we detect interactions by considering intermediate layers individually. We were only able to detect interactions by considering strongly weighted paths entering the first hidden layer.

We guess that a neural network mainly uses its early hidden layers to model interactions and its later layers to model the nonlinearities of these interactions. We leave an investigation into this interpretation for future work.

Feature Correlations Correlations between features can complicate the task of detecting interactions because if features are correlated, any interaction involving one of the features is

also involved in the correlated feature. A common problem in interaction detection (Sorokina et al., 2008b; Lou et al., 2013), this scenario would prevent interaction detection methods from approximating interaction strength well because each of the correlated features would accrue a portion of interaction strength, thereby obfuscating the true interaction strength with either feature.

The issue of feature correlations can be mitigated in part by selected highly correlated features and removing them, so long as their removal does not significantly decrease a model’s predictive performance (Sorokina et al., 2008b).

4 Interaction Detection

In this section, we propose our feature interaction detection algorithm NID, which can extract interactions of all orders without individually testing for each of them. Our algorithm is composed of three main steps: 1) obtain an initial list of interactions; 2) rank the interactions based on their strength; 3) determine a cut-off for the top K interactions.

These three steps of the NID algorithm are meant to address the following challenges associated with detecting interactions of arbitrary order: 1) a search over an exponential solution space of all 2^p possible interactions is prohibitively expensive, and testing for all interactions can result in many false positives; 2) the ranking of interactions cannot be biased to higher or lower-order interactions, therefore interactions of different orders must be ranked on the same scale; and 3) even with an accurate ranking of interaction candidates, the practical utility of NID still requires the non-trivial task of determining a cut-off between meaningful and spurious interactions.

4.1 Greedy Initial Interaction Selection

In the first stage of our algorithm, we propose a list of potential interactions from learned weight matrices, where our goal is to achieve high recall. We propose a set of interactions by examining individual hidden units in the first layer based on each of their corresponding rows \mathbf{w}' in the first weight matrix.

For this weight vector \mathbf{w}' , it is natural to propose any set of features with nonzero weight as an interaction. However, this approach generates interactions between many features since \mathbf{w}' can contain many nonzero values even after applying an L1 penalty. To obtain an acceptable list of interaction candidates, the magnitude of the weights must be considered. One simple solution is to truncate the weight vector by a threshold; however, there is no principled way to select an optimal threshold, and a suboptimal threshold can cause true interactions to be overlooked.

To remedy the above issues, we adopt the following greedy procedure for proposing interactions. Let i_1, i_2, \dots, i_p be a permutation of $[p]$ that sorts $|\mathbf{w}'|$ in descending order, i.e., $|w'_{i_1}| \geq |w'_{i_2}| \geq \dots |w'_{i_p}|$. We propose $p - 1$ potential interactions $\mathcal{I}'_j, \forall j = 2, \dots, p$, where $\mathcal{I}'_j = \{i_1, i_2, \dots, i_j\}$. This approach is equivalent to truncating the weight vector \mathbf{w}' with all possible thresholds and selecting features with nonzero weights as interactions.

This greedy strategy has the following advantages: 1) it filters a locally optimal set of interaction candidates by considering those candidates with the highest weights entering individual hidden units, 2) the strategy is designed to select more interaction candidates than the true number of interactions, and 3) the selection procedure prevents the need for searching an exponential solution space of interaction candidates. After greedy selection, there are at most

$(p-1)p_1$ interactions proposed, which is significantly smaller than the initial 2^p . Our empirical study in Section 5 suggests that our greedy initial interaction selection rarely misses true interactions.

4.2 Ranking Selected Interactions

With an initial list of interactions $\{\mathcal{I}_i\}_{i=1}^m$, we proceed to rank them based on their importance. Namely, we rank the list using interaction strength, a measure defined in Section 3.3. A simple solution to ranking interactions is to aggregate the strengths of each interaction over the entire first hidden layer. In other words, for a potential interaction \mathcal{I} , we calculate its importance $w(\mathcal{I})$ as $\sum_{i=1}^{p_1} \omega_i(\mathcal{I})$. However, using this formulation, the ranking will be biased towards lower-order interactions. For example, let us consider a 3rd-order interaction $\{1, 2, 3\}$. Since it subsumes three pairwise interactions $\{1, 2\}, \{2, 3\}$ and $\{1, 3\}$, they are very likely to also be included in the initial list. Take $\{1, 2\}$ as an example. We have that $\omega_i(\{1, 2\}) \geq \omega_i(\{1, 2, 3\})$ for any $i \in [p_1]$ since $\omega_i(\mathcal{I})$ is defined as the minimum weight within \mathcal{I} . As a result, the higher-order interaction tends to be ranked after the lower-order interactions it encapsulates, which is not a desirable property.

We address this problem by re-examining the hidden units that proposed interaction \mathcal{I} from the *greedy selection stage*. Concretely, a potential interaction \mathcal{I} can be proposed by multiple hidden units $\mathcal{S}_{\mathcal{I}} \subseteq [p_1]$. When evaluating the importance of \mathcal{I} , we only aggregate the hidden units in $\mathcal{S}_{\mathcal{I}}$, i.e., $w(\mathcal{I}) = \sum_{i \in \mathcal{S}_{\mathcal{I}}} \omega_i(\mathcal{I})$. Such an aggregation has numerous benefits for ranking interaction candidates, especially when comparing interactions of different orders. First, an important interaction can be traced to multiple hidden units with significant strength, which leads to a higher ranking. Moreover, for spurious interactions that are proposed by a small number of hidden units, their importance is limited to those hidden units alone, effectively decreasing their ranking.

The aggregation has a special property that improves the rankings of interactions of different orders. Recall the previous example with a 3rd-order interaction $\{1, 2, 3\}$. If the interaction of $\{1, 2\}$ only exists as a by-product of interaction $\{1, 2, 3\}$, the hidden unit origin of $\{1, 2\}$ will be a subset of that of $\{1, 2, 3\}$, i.e., $\mathcal{S}_{\{1, 2\}} \subseteq \mathcal{S}_{\{1, 2, 3\}}$. When there are several of such subsets of the same higher-order interaction, then the ranking of the higher-order interaction improves, which we prove below under mild assumptions.

Theorem 4 (Improving the ranking of high-order interactions). *Let \mathcal{R} be the set of interactions proposed by Algorithm 1, let $\mathcal{I} \in \mathcal{R}$ be a high order interaction of order d where $d \geq 3$, and let \mathcal{S} be the set of subset interactions of \mathcal{I} of order $d-1$ where $|\mathcal{S}| = d$. Assume that for any hidden unit j which proposed $s \in \mathcal{S} \cap \mathcal{R}$, \mathcal{I} will also be proposed at the same hidden unit, and $w_j(\mathcal{I}) > \frac{1}{d}w_j(s)$. Then, one of the following must be true: a) $\exists s \in \mathcal{S} \cap \mathcal{R}$ ranked lower than \mathcal{I} , i.e., $w(\mathcal{I}) > w(s)$, or b) $\exists s \in \mathcal{S}$ where $s \notin \mathcal{R}$.*

Proof. Suppose for the purpose of contradiction that $\mathcal{S} \subseteq \mathcal{R}$ and $\forall s \in \mathcal{S}, w(s) \geq w(\mathcal{I})$. Because $w_j(\mathcal{I}) > \frac{1}{d}w_j(s)$,

$$w(\mathcal{I}) = \sum_{s \in \mathcal{S} \cap \mathcal{R}} \sum_{j \text{ propose } s} z_j w_j(\mathcal{I}) > \frac{1}{d} \sum_{s \in \mathcal{S} \cap \mathcal{R}} \sum_{j \text{ propose } s} z_j w_j(s) = \frac{1}{d} \sum_{s \in \mathcal{S} \cap \mathcal{R}} w(s).$$

Since $\forall s \in \mathcal{S}, w(s) \geq w(\mathcal{I})$,

Algorithm 1 NID Greedy Ranking Algorithm

Input: input-to-first hidden layer weights $\mathbf{W}^{(1)}$, aggregated weights $\mathbf{z}^{(1)}$

Output: ranked list of interaction candidates $\{\mathcal{I}_i\}_{i=1}^m$

- 1: $d \leftarrow$ initialize an empty dictionary mapping interaction candidate to interaction strength
 - 2: **for** each row \mathbf{w}' of $\mathbf{W}^{(1)}$ indexed by r **do**
 - 3: **for** $j = 2$ to p **do**
 - 4: $\mathcal{I} \leftarrow$ sorted indices of top j weights in \mathbf{w}'
 - 5: $d[\mathcal{I}] \leftarrow d[\mathcal{I}] + z_r^{(1)} \min_{i \in \mathcal{I}} \{w'_i\}$
 - 6: $\{\mathcal{I}_i\}_{i=1}^m \leftarrow$ interaction candidates in d sorted by their strengths in descending order
-

$$\frac{1}{d} \sum_{s \in \mathcal{S} \cap \mathcal{R}} w(s) \geq \frac{1}{d} \sum_{s \in \mathcal{S} \cap \mathcal{R}} w(\mathcal{I})$$

Since $\mathcal{S} \subseteq \mathcal{R}$, $|\mathcal{S} \cap \mathcal{R}| = d$. Therefore,

$$\frac{1}{d} \sum_{s \in \mathcal{S} \cap \mathcal{R}} w(\mathcal{I}) \geq \frac{1}{d} w(\mathcal{I}) d \geq w(\mathcal{I}),$$

which is a contradiction. \square

Under the noted assumption, Theorem 4 part a) shows that a d -order interaction will improve over one its $d - 1$ constituents in rankings as long as there is no sudden drop from the weight of the $(d - 1)$ -order to the d -order interaction at the same hidden units. We note that the improvement extends to b) as well, when $d = |\mathcal{S} \cap \mathcal{R}| > 1$. By improving the ranking of a high-order interaction over its subset interactions, the high-order interaction can be captured earlier in the cutoff stage (described in the next section), and it has a better chance of ranking above any false positives.

In summary, we rank the interactions in the initial list by their respective interaction strengths. We denote the ranked list by $(\mathcal{I}_1, \mathcal{I}_2, \dots, \mathcal{I}_m)$, where $\omega(\mathcal{I}_1) \geq \omega(\mathcal{I}_2) \geq \dots \geq \omega(\mathcal{I}_m)$. Before presenting the final ranked list, we prune it to remove redundant interactions that are subsets of higher ranked interactions. For example, when $\{1, 2, 3\}$ is ranked higher than $\{1, 2\}$, we remove $\{1, 2\}$.

In our empirical study on synthetic data, we observed that our ranking is highly informative, where true interactions rank at the top of the candidate list. The procedures for *greedy selection* and *interaction ranking* are summarized in combined form as Algorithm 1.

4.3 Cut-off on Interaction Ranking

The ranked list of interaction candidates provides valuable information on their relative ordering; however, there may be a need to identify true interactions instead of only providing a ranked list. Thus, we need a way to “cut off” the ranked list, so we can predict true top- K interactions, $\{\mathcal{I}_i\}_{i=1}^K$.

We propose a method of identifying such interactions by training a special form of *generalized additive model (GAM)* that incorporates arbitrary-order interactions as additive terms, and

evaluating predictive performance on a validation set. The *GAM* we train is neural network-based, where each additive term is a separate neural network, and together the neural networks are summed at their outputs. This neural network-based *GAM* leverages the joint training capabilities of backpropagation to efficiently construct the additive model.

Moreover, this *GAM* utilizes the representational power of neural networks. Therefore, we expect that when this model incorporates highly ranked interactions, it will yield predictive performance on par with that of the neural network we originally interpreted.

To cut off the ranked list of interactions, we gradually increase K until *GAM* performance on the validation set plateaus, then report $\{\mathcal{I}_i\}_{i=1}^K$ as the identified interactions among features. Namely, for the set of interactions $\{\mathcal{I}_i\}_{i=1}^K$, we design the additive model $f_K(\mathbf{x})$:

$$f_K(\mathbf{x}) = \sum_{i=1}^p g_i(x_i) + \sum_{i=1}^K g'_i(\mathbf{x}_{\mathcal{I}}),$$

where $g_i(\cdot)$ captures the main effects and $g'_i(\cdot)$ captures the interactions.

4.4 Pairwise Interaction Detection

Our algorithm can also be easily adjusted for pairwise interaction detection. Pairwise interaction detection has been a canonical problem in interaction detection literature (Lou et al., 2013; Fan et al., 2016) due to its simplicity. Modeling pairwise interactions is also the *de facto* objective of many successful machine learning algorithms such as factorization machines (Rendle, 2010) and hierarchical lasso (Bien et al., 2013).

We rank all pairs of features $\{i, j\}$ according to their interaction strengths $\omega(\{i, j\})$ calculated on the first hidden layer, where

$$\omega(\{i, j\}) = \sum_{s=1}^{p_1} \omega_s(\{i, j\}).$$

The higher the rank, the more likely the interaction exists.

5 Experiments

To demonstrate our framework, we evaluate interactions detected on synthetic datasets, analyze interactions discovered on real-world datasets, and provide a runtime analysis on all datasets.

5.1 Experimental Setup

Neural Network Configuration In our experiments, we trained a multilayer neural network with one component to model feature interactions, and separate components to model main effects (see Figure 2). The interaction and main effect components are summed at their outputs to enable joint training via backpropagation. The input dimension of the feature interaction component is the total number of features, p , and the input dimensions of each of the main effect components is 1.

In all of our experiments, the feature interaction component of our neural network consisted of four hidden layers with first-to-last layer sizes of: 140, 100, 60, and 20 hidden units. The main effects components each had three hidden layers with sizes of: 10, 10 and 10 hidden units. All layers in all of our networks used ReLU activation. The learning objectives used were: minimizing mean-squared error for regression tasks, and minimizing softmax cross-entropy for

Table 1: Functions F_1 - F_4 for generating synthetic data.

$F_1(\mathbf{x})$	$\pi^{x_1 x_2} \sqrt{2x_3} - \sin^{-1}(x_4) + \log(x_3 + x_5) - \frac{x_9}{x_{10}} \sqrt{\frac{x_7}{x_8}} - x_2 x_7$
$F_2(\mathbf{x})$	$\exp x_1 - x_2 + x_2 x_3 - x_3^{2 x_4 } + (x_1 x_4)^2 + \log(x_4^2 + x_5^2 + x_7^2 + x_8^2) + x_9 + \frac{1}{1 + x_{10}^2}$
$F_3(\mathbf{x})$	$x_1 x_2 + x_2 x_3 + x_3 x_4 + x_4 x_5 + x_5 x_1$
$F_4(\mathbf{x})$	$x_1 x_2 + x_1 x_3 + x_2 x_3 + x_1 x_4 + x_5$

Table 2: AUC of pairwise interaction strength from various interaction detection methods on synthetic data.

	NID (proposed)	ANOVA	HierLasso	AG
$F_1(\mathbf{x})$	0.995	0.992	1.00	0.983
$F_2(\mathbf{x})$	0.996	0.563	0.634	0.999
$F_3(\mathbf{x})$	1.00	1.00	1.00	1.00
$F_4(\mathbf{x})$	1.00	1.00	1.00	1.00

classification tasks. The L1 constants we used range from 5e-6 to 5e-4. In each experiment, the neural network is trained once to fit data, then we use our interaction ranking algorithms to extract feature interactions from network weights.

Synthetic Data We evaluate the interactions detected by NID on four synthetic datasets generated by functions listed in Table 1. Each of the four datasets had a training/valid/test of 1/3 each on 30k data points. The data from functions F_2 to F_4 are uniformly distributed between -1 and 1, and the data from F_1 are uniformly distributed with the same variable ranges used by Sorokina et al. (2008b). We select the four functions F_1 to F_4 for their desirable properties in evaluating interaction detection methods. F_1 has a combination of strong and weak interaction terms of varying order and nonlinearity, and this function has been studied frequently among interaction detection methods (Hooker, 2004; Sorokina et al., 2008b; Lou et al., 2013). F_2 is designed to have symmetry along the y -axis to test NID’s ability to model interactions that are highly nonlinear. F_3 is designed to have a ring structure, where all variables are linked in a circular chain based on their pairwise interactions, so we can test NID’s ability to avoid modeling spurious interactions between other combinations of variables. Finally, F_4 contains a clique between x_1 , x_2 , and x_3 , where all three variables are interlinked by pairwise interactions, but they do not form a 3rd-order interaction.

In our experiments, we include another synthetic dataset, *kin8nm*, which consists of 8.2k data points (Rasmussen et al., 2003). *kin8nm* describes a noisy simulated movement of a robotic arm based on joint angles, which are features in the dataset. The features are inputted into a forward kinematics computation, which transforms among coordination systems of each joint to compute the position and orientation of an end-effector. For this dataset, we use the same 80/10/10 train/valid/test split ratio used in Sorokina et al. (2008b).

Real-world Data We apply NID on three real-world datasets and compare our results on two of the datasets with findings from past studies. All three datasets underwent feature selection/removal to assist in removing potential feature correlations. We used selection criteria from (Sorokina et al., 2008b) to decide which features to remove for the first two datasets. For the third dataset on identifying the Higgs Boson, we remove features that have high distance

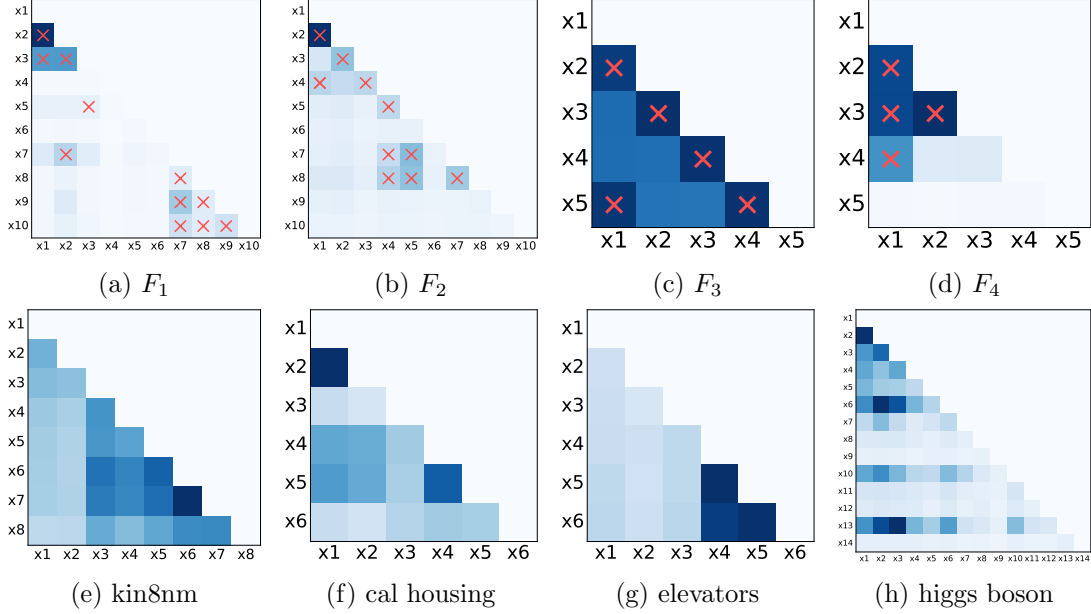


Figure 3: Pairwise interaction strengths generated by NID for synthetic and real-world datasets. Red cross-marks indicate ground truth for synthetic datasets.

correlation (Székely et al., 2007) with all other variables and whose removal does not reduce classification accuracy by more than 0.2%. All three real-world datasets had a train/valid/test split ratio of 80/10/10, and this ratio is consistent with past studies (Sorokina et al., 2008b).

The real-world datasets we use are described as follows. The California Housing dataset (Pace & Barry, 1997) is a regression dataset with 21k data points for predicting California housing prices. The Elevators dataset (Camachol, 1998) is a regression dataset with 17k data points for describing the control of an aircraft. The Higgs Boson dataset (Adam-Bourdarios et al., 2014) comes from the Higgs Boson Machine Learning challenge hosted on Kaggle. This dataset has 250k data points and is used to classify whether a particle environment originates from the decay of a Higgs Boson.

Baselines We compare the performance of NID to that of three baseline algorithms. Two-Way *ANOVA* (Wonnacott & Wonnacott, 1972) utilizes linear models to conduct significance tests on the existence of interaction terms. *Hierarchical lasso* (HierLasso) (Bien et al., 2013) applies lasso feature selection to extract pairwise interactions. *Additive Groves* (AG) (Sorokina et al., 2008b) is a nonparametric method of testing interactions of arbitrary order by placing structural constraints on an additive model of regression trees.

5.2 Pairwise Interaction Detection

As discussed in Section 4.4, our algorithm can be used for pairwise interaction detection. The results of pairwise interaction detection are shown in Figure 3. Heat-maps show the relative strengths of all pairwise interactions. Ground truth is indicated by red cross-marks. As shown in the heat-maps, NID has consistently high interaction strengths at the cross-marks relative to other interaction candidates. This assessment is quantified in Table 2. The AUC score for NID and each baseline is shown for pairwise interaction detection for the four synthetic

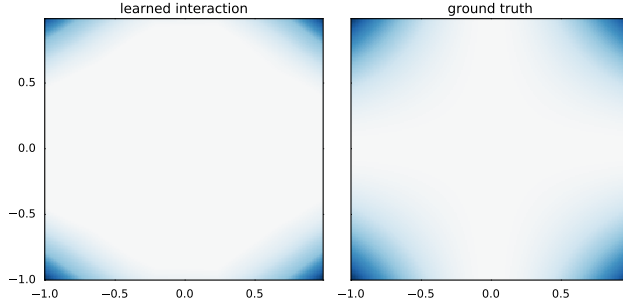


Figure 4: A heatmap comparison for the $(x_1x_4)^2$ interaction in F_2 . The left heatmap is learned by our additive model used in the cutoff stage of NID.

datasets generated by the functions in Table 1. For NID and *AG*, we ran ten trials of pairwise interaction detection on each dataset and removed the trials with the highest and lowest AUC scores. For each function F_1 to F_4 , NID performs near perfectly, providing strong support that our algorithm can rank interactions accurately and consistently even when the interactions have significant nonlinearity. In comparison to baseline methods, our method outperforms *ANOVA* and *HierLasso* on data generated by F_2 . This is expected because interactions that are symmetric around the y -axis (nonlinear) are very difficult for linear functions to approximate. Our algorithm performs better or comparable to *AG*, but the difference is not significant since they are both accurate. We exclude the synthetic dataset, *kin8nm*, from Figure 3 and Table 1 because all 8 features in the dataset are interacting.

5.3 Arbitrary-order Interaction Detection

We apply NID to the problem of arbitrary-order interaction detection on all 8 datasets. For each dataset, our algorithm produces a ranked list of interactions ordered by decreasing strength. We also apply a cutoff on each ranked list to distinguish true interactions predicted by NID. We provide evidence that the model responsible for cutoff, as discussed in Section 4.3, indeed trains properly. In Figure 4, two heatmaps compare plots for the same learned and ground truth interaction from synthetic function F_2 . The similarity between plots suggest that the cutoff model, when correctly structured, can indeed learn interactions as expected even when the interaction is weak, such as the case of $(x_1x_4)^2$ from F_2 (Figure 5b).

Synthetic data The results of running our algorithm for arbitrary-order interaction detection are summarized in Figure 5. The performance of NID is highly accurate for the synthetic data generated by F_1 and F_2 . Most notably, our method correctly ranks high order interactions. In particular, NID correctly found a weak 4th-order $\{7, 8, 9, 10\}$ interaction from F_1 when *AG* could not (Sorokina et al., 2008b).

Besides correctly ranking higher-order interactions, the cutoff strategy we developed shows signs of being robust to false positives and negatives in interaction rankings. For example, for F_1 , our algorithm inadvertently screens an interaction between x_3 and x_5 , which is known to be weak (Sorokina et al., 2008b), nevertheless the additive model correctly cuts the ranking right after the second weakest interaction between x_2 and x_7 . For F_2 , the cutoff model continues to search for the last true interaction despite encountering a false positive $\{1, 2, 3\}$ before it.

The ring and clique structures of F_3 and F_4 pose great challenges for higher-order interaction detection as it is more difficult to separate pairwise interactions from higher-order interactions. For example, while our method correctly ranks two of the 5 pairwise interactions of F_3 correctly

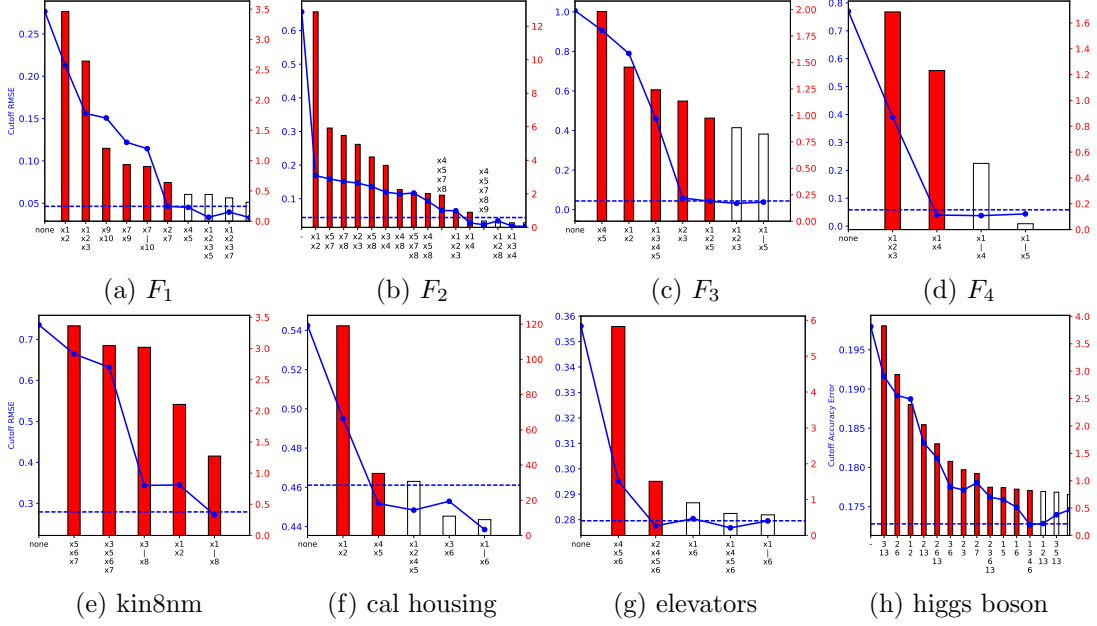


Figure 5: The behaviors of NID’s interaction ranking (red) and cutoff (blue) when detecting arbitrary-order interactions on synthetic and real-world datasets. The x -axis of each plot shows non-exhaustive shortlists of top interaction candidates generated by NID. Interaction strengths are represented by the red bars, and the solid blue curves are cutoff curves that begin at the x -label, “none” or “-”, corresponding to the *main effects*. Predictive performance improves as interaction terms are added into the cutoff model, shown by the blue curve. In this case, cutoff occurs after the cutoff model surpasses NID’s original prediction performance, marked by the dashed blue lines.

at the top, the next interaction in the ranking is a false 4th-order interaction. For experiments on the 3-way clique structure of F_4 , the neural network cannot separate the clique at all, causing NID to falsely detect a $\{1, 2, 3\}$ interaction.

Our results on synthetic data show that our approach can outperform the state-of-the-art in high-order interaction detection. In addition to outperforming *AG* in detecting the $\{7, 8, 9, 10\}$ interaction from F_1 , our method also finds an 8-th order interaction between all features in the *kin8nm* dataset. Although *AG* reports only a subset of the 8 features as interacting (Sorokina et al., 2008b), strong support for the existence of the 8th-order interaction comes from the forward kinematics equation (Murray et al., 1994) that generated the dataset. This equation computes coordinate transformations for all 8 joint angle features, so every joint angle must be interacting even if their combined interaction strength is weak.

Real-world data On real-world datasets, the interactions detected by our method are consistent with the findings of Sorokina et al. (2008b). For example, NID identifies x_1, x_2 and x_4, x_5 in the California Housing dataset and a 3rd-order interaction between x_4, x_5 , and x_6 in the Elevators dataset. This consistency suggests that our method can be used to detect interactions in real-world data.

In the Higgs Boson dataset, three types of particles are of interest for detecting the decay of a Higgs Boson: hadronic taus, leptons, and neutrinos. Our algorithm identifies two 4th-order

Table 3: Definitions of individual variables (Adam-Bourdarios et al., 2014) that constitute the 4th-order interactions detected by NID: $\{2, 3, 6, 13\}$ and $\{1, 3, 4, 6\}$.

x_1	The transverse mass between the missing transverse energy and the lepton
x_2	The invariant mass of the hadronic tau and the lepton
x_3	The R separation between the hadronic tau and the lepton
x_4	The modulus of the vector sum of the missing transverse momenta and the transverse momenta of the hadronic tau, the lepton, the leading jet and the subleading jet
x_6	The centrality of the azimuthal angle of the missing transverse energy vector with respect to the hadronic tau and the lepton
x_{13}	The missing transverse energy E_{miss}

interactions in the Higgs Boson Dataset associated with key properties of the three particles. From Figure 5e, we can see that the two 4th-order interactions are the interactions between x_2, x_3, x_6 , and x_{13} and between x_1, x_3, x_4 , and x_6 . See Table 3 for the definitions of these variables. For the first 4th-order interaction, the features x_2, x_3 , and x_6 are derived properties of a hadronic tau and a lepton, and x_{13} is a property of neutrinos (Adam-Bourdarios et al., 2014). In fact, missing transverse energy x_{13} is the only feature of neutrinos, the most illusive particle in detecting the decay of a Higgs Boson. We suspect a 4th-order interaction because these features describe important properties of decay particles and interlink some or all three of the particles, which are important combinations for detecting the Higgs Boson (Jakobs & Seez, 2016).

The $\{1, 3, 4, 6\}$ interaction term is an interaction amongst the same definitions of x_3 and x_6 , as well as the transverse mass between the missing transverse energy and the lepton (x_1), and the modulus of the missing transverse momenta and the transverse momenta of the hadronic tau, the lepton, and leading and subleading jets (x_4). We suspect that this 4th-order interaction is detected because it seems to describe the joint kinematics of the 3 decay particles.

5.4 Empirical Evaluation of Greedy Algorithm 1

Efficiency

One of the practical advantages of using NID for interaction detection compared to other methods is its ability to detect arbitrary-order interactions without searching through an exponential number of interaction candidates. To show the runtime advantage of our framework against a competing interaction detection method, we compare our framework’s runtime to that of the Additive Groves (AG), which is to the best of our knowledge, the state-of-the-art for arbitrary-order interaction detection that does not restrict the form of detected interactions. Figure 6 shows a comparison of runtimes between our framework and AG for all eight datasets. We show the runtimes of arbitrary order interaction detection using the following three methods: AG , our NID framework with cutoff, and our NID ranking algorithm without cutoff. All runtime experiments with AG involved no hyperparameter tuning, and to save time, we followed the practical advice of Sorokina et al. (2008b) to only test interaction candidates with gradually increasing orders when those candidates were already found as cliques at previous orders.

The result of our runtime experiments show that NID interaction ranking without cutoff

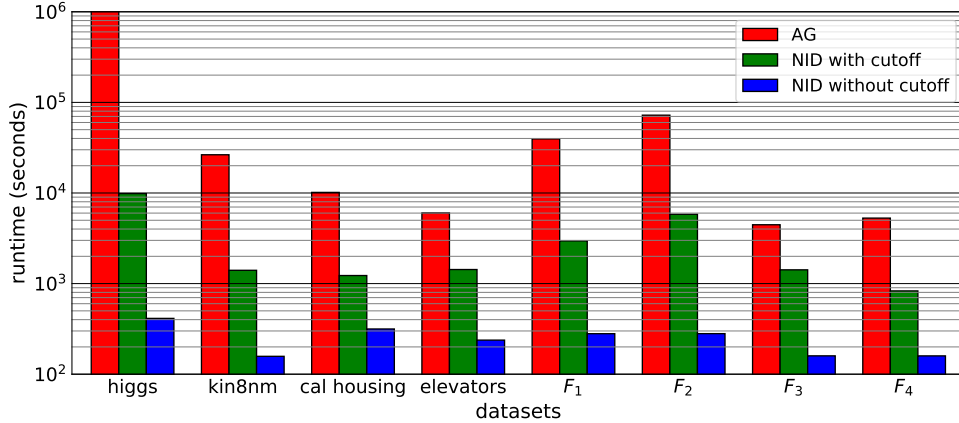


Figure 6: Comparison between the running times of *AG*, *NID* with cutoff, and *NID* without cutoff. The runtime limit is set to be 10^6 seconds or 11.6 days.

consistently takes no more than seven minutes, or about the same time it takes to train our neural network architecture. Compared to *AG*, the same interaction ranking algorithm performs at least an order of magnitude faster when the number of features is small (e.g. six or less), but it begins to perform several orders of magnitude faster than *AG* when the number of features is greater or equal to eight. The same story of increasing runtime discrepancy applies to our interaction detection framework *with* cutoff as well. Across our experiments, the framework was often faster than *AG* by an order of magnitude, but for the Higgs Boson dataset (*higgs*) with 14 features, our framework with cutoff was at least two orders of magnitude faster (2.8 hours versus 11.6 days). We capped the runtime of our experiments at 10^6 seconds, and *AG* exceeded this time limit in the *higgs* experiment.

The runtimes also depend on dataset size, since the training time of machine learning models depends on how much data they learn from. In those cases where *NID*-ranking *without* cutoff was faster than *AG* by one or two orders of magnitude, the size of datasets was on the order of 10^4 data points, and in the case of the *higgs* experiment, the dataset size was 250k, which increased running times of all compared methods.

Ranking Quality

We develop a test suite of complex functions to empirically evaluate the quality of interaction rankings generated by *NID* and *AG*. Both *NID* and *AG* rely on high quality interaction rankings for accurate interaction detection, but they have different approaches to ranking interactions. In the case of our framework, we use interaction strength (defined in Section 3) to generate rankings (described in Section 4.1). By contrast, *AG* uses a standard deviation measure as a proxy for “interaction strength”. *AG* computes the difference between two models: an unrestricted additive model of regression trees, and the same model but restricted of the interaction in question. The difference in performance is then compared to a hard cutoff of 3 standard deviations of model variability; that is, when the restricted model performs at least 3 standard deviations worse than the unrestricted model, the interaction is said to exist. Thus, the “interaction strength” of *AG* is the number of standard deviations of performance drop by each restricted model.

Our test suite consists of ten complex functions that contain four arbitrary-order interactions

Table 4: Tests with complex data-generating functions used to benchmark the performance of *AG* and *NID*, where the results for different averaging methods in *NID* are shown. Refer to Section 3.1 and Algorithm 1 for how averaging methods are incorporated into *NID*. Each score counts how many true top-ranked interactions are generated by each method before any false positive is ranked. *max.* stands for maximum value, *r.m.s.* stands for root mean square, *arith.* stands for arithmetic mean, *geom.* stands for geometric mean, *harm.* stands for harmonic mean, and *min.* stands for minimum value.

test	data generating functions	<i>AG</i>	<i>NID</i>					
			<i>max.</i>	<i>r.m.s.</i>	<i>arith.</i>	<i>geom.</i>	<i>harm.</i>	<i>min.</i>
T_1	$\exp(x_1 - x_2) + x_2 x_3 - (x_3^2)^{ x_4 } + \frac{1}{\log(x_4^2 + x_5^2 + x_7^2 + x_8^2) + x_9 + \frac{1}{1 + x_{10}^2}}$	4/4	0/4	0/4	1/4	3/4	4/4	4/4
T_2	$\pi^{x_1 x_2} \sqrt{2 x_3 } + \log(x_3 + x_5 + 1) - x_2 x_7 + \frac{x_9}{1 + x_{10} } \sqrt{\frac{x_7}{1 + x_8 }} - \arcsin(0.5x_4)$	3/4	0/4	0/4	1/4	0/4	0/4	2/4
T_3	$\min(x_1, x_2) - 10 x_3 + (x_1 x_4)^2 - \arctan(x_5 x_6 x_7) + (x_6 + x_7 + x_8 + x_9 + x_{10})^2$	1/4	0/4	1/4	1/4	4/4	4/4	4/4
T_4	$\frac{1}{1 + x_1^2 + x_2^2 + x_3^2} + \sqrt{\exp(x_4 + x_5) + x_6 + x_7 + x_8 x_9 x_{10}}$	2/4	0/4	0/4	2/4	3/4	3/4	3/4
T_5	$\exp(x_1 x_2 + 1) - \exp(x_3 + x_4 + 1) + \cos(x_5 + x_6 - x_8) + \sqrt{x_8^2 + x_9^2 + x_{10}^2}$	2/4	0/4	1/4	1/4	2/4	3/4	3/4
T_6	$(\arctan(x_1) + \arctan(x_2))^2 + \max(x_3 x_4 + x_6, 0) - \frac{1}{1 + (x_4 x_5 x_6 x_7 x_8)^2} + \left(\frac{ x_7 }{1 + x_9 }\right)^5 + \sum_{i=1}^{10} x_i$	3/4	0/4	0/4	1/4	3/4	3/4	3/4
T_7	$x_1 x_2 + 2^{x_3 + x_5 + x_6} + 2^{x_3 + x_4 + x_5 + x_7} + \sin(x_7 \sin(x_8 + x_9)) + \arccos(0.9x_{10})$	1/4	0/4	0/4	1/4	1/4	1/4	3/4
T_8	$(x_1 - x_2 + x_3 - x_4)^2 + x_4 x_6 x_8 - \arcsin(0.95 \max(x_5, x_6)) + \sqrt[3]{ x_7 + x_8 }$	3/4	0/4	0/4	2/4	3/4	3/4	3/4
T_9	$\tanh(x_1 x_2 + x_3 x_4) \sqrt{ x_5 } + \exp(x_5 + x_6) + \log((x_6 x_7 x_8)^2 + 1) + x_9 x_{10} + \frac{1}{1 + x_{10} }$	2/4	0/4	0/4	2/4	2/4	3/4	3/4
T_{10}	$\sinh(x_1 + x_2) + \arccos(\tanh(x_3 + x_5 + x_7)) + \cos(x_4 + x_5) + \sec(x_7 x_9)$	4/4	0/4	0/4	2/4	3/4	4/4	4/4
total		25/40	0/40	2/40	14/40	21/40	28/40	32/40

each, and several of the functions also include main effects. The interactions have various forms of nonlinearities, and in multiple tests, we design functions where interacting features partially overlap. All datasets generated by the functions consist of 10 features and 20k data points, where half of the data set is used for training, and the other half is used for testing. Every x_i in all tests is generated from a uniform distribution between -1 and 1 .

We evaluate the performance of interaction detection methods by counting how many top-ranked interactions generated by each method are true interactions before any false positive is ranked. Thus, there can never be more than four correct in each test score. Then, we count up total scores for each method over all tests. We do not count any constituent of a true interaction as a false positive, but the constituents do not count towards the scores. Table 4 shows the results of this evaluating on different methods. Scores for *AG* and *NID* are shown. For *NID*, we further show the performance of different averaging methods when they are incorporated into the framework. See Section 3.1 for an explanation of this comparison.

Details on the test configurations of each model are as follows. For NID, we interpret a neural network with four hidden layers with hidden unit counts of 140, 100, 60, and 20 starting from first to last hidden layer. Main effect branches are added to the output of each neural network (see Appendix 3.4 under “Modeling Main Effect”). Each branch consists of three hidden layers with 10 hidden units in each layer. An L1 penalty (see Appendix 3.4 under “Sparsity-inducing Penalty”) of 5e-5 was used. The training objective is to minimize mean-squared error. After training a neural network to fit to data, we directly interpret its interaction ranking. We train each network with the same configurations over all tests.

For *AG*, we train each grove model in “layered-mode” for interaction detection, as recommended by *AG*’s original documentation in the *TreeExtra* package¹. We use default hyperparameters for every model. Like our runtime analysis on *AG*, we follow the practical advice of Sorokina et al. (2008b) to search for interaction candidates in a Breadth First Search-like manner, where we only test for a d -order interaction when all of its $(d - 1)$ -interactions were already tested to exist. By using this approach to testing interactions, we must test for all pairwise interactions first, which is done by default in the *TreeExtra* implementation.

As shown in Table 4, when using either the minimum value or harmonic mean averaging (or aggregating) methods, NID was able to detect more top-ranked interactions free of false positives than could *AG*. Moreover, minimum value in NID outperformed all other averaging methods. A clear trend can be seen where the more minimum-dominant a mean is, the more true top-ranked interactions are recovered before any false positive. Note that all averaging methods considered are representative of the generalized mean family Bullen et al. (1988).

5.5 Visualizing Interactions Starting at Hidden Layers

In addition to detecting feature interactions, we apply NID to detecting interactions between hidden units. Specifically, we apply NID to each hidden layer in the neural networks we previously studied except for the last hidden layer, since our interaction detection algorithm requires that there is at least one hidden layer between the layer of interest and the final output. We visualize the statistical interactions detected by NID from hidden layers in Figures 7 and 8. These visualizations show the interactions represented by different edge colors, where each node is a hidden unit (or input feature for the top-left grids), and each edge is a pairwise interacting correspondence between two of the nodes. Note that all detected interactions that are subsets of other detected interactions are excluded from the visualizations. Since some visualizations can be difficult to interpret, we directly list the interactions that generated them in Table 5.

A common trend from the visualizations in Figures 7 and 8 is observing that interactions originating at first hidden layers are very high-order in general, whereas interactions originating at later layers are much lower-order. In order to further investigate this observation, we reran experiments on a neural network architecture that had 100 hidden units at every hidden layer rather than the pyramid architecture in our experiments (e.g. Figure 2). Even when fixing the number of the hidden units at every hidden layer, the same trend still holds where first hidden layer interactions have the highest orders in general, as shown in Figure 9. Moreover, the highest order of detected interactions tends to decay quickly when considering later hidden layers of origination.

Visualizing interaction behavior starting at different hidden layers may be useful for setting a guideline on neural network architecture design, e.g. how many hidden layers and hidden units a fully-connected neural network needs to fit well to a specific dataset. Moreover, having an understanding of interacting components in a neural network could be useful for model editing, e.g. disentangling the neural network.

¹http://additivegroves.net/AG_interactions.htm

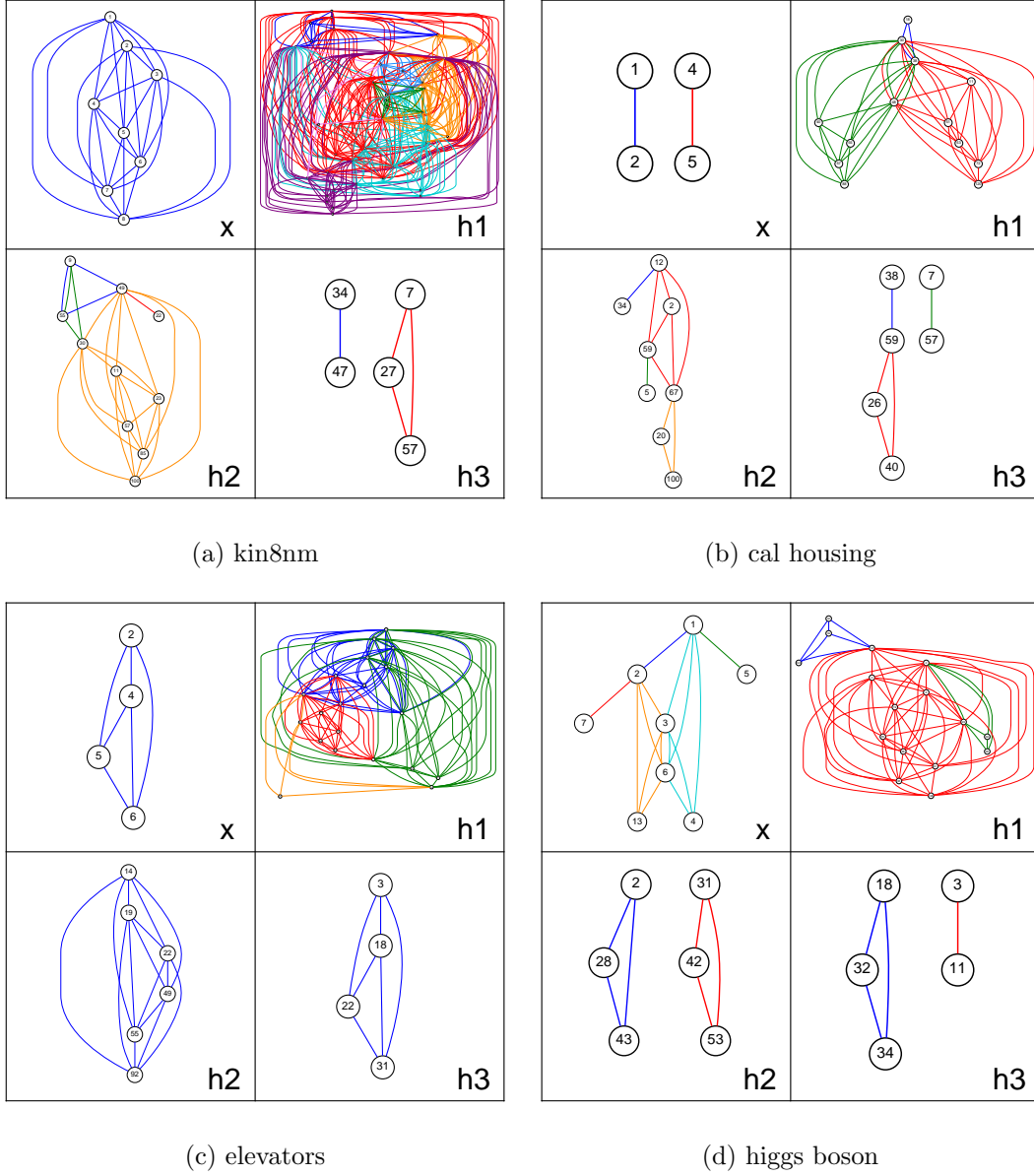


Figure 7: Visualization of interactions detected by NID at input layer, “x”, and hidden layers, “h1”, “h2”, and “h3” for real-world datasets and the simulated *kin8nm* dataset. Different edge colors represent distinct interactions that are not subsets of other detected interactions. Nodes represent hidden units in the cases of h1-h3 or input features in the case of x, and edges represent pairwise correspondence between nodes as part of the interaction represented by edge color. Refer to Section 5.1 for the neural network architecture that NID was applied to.

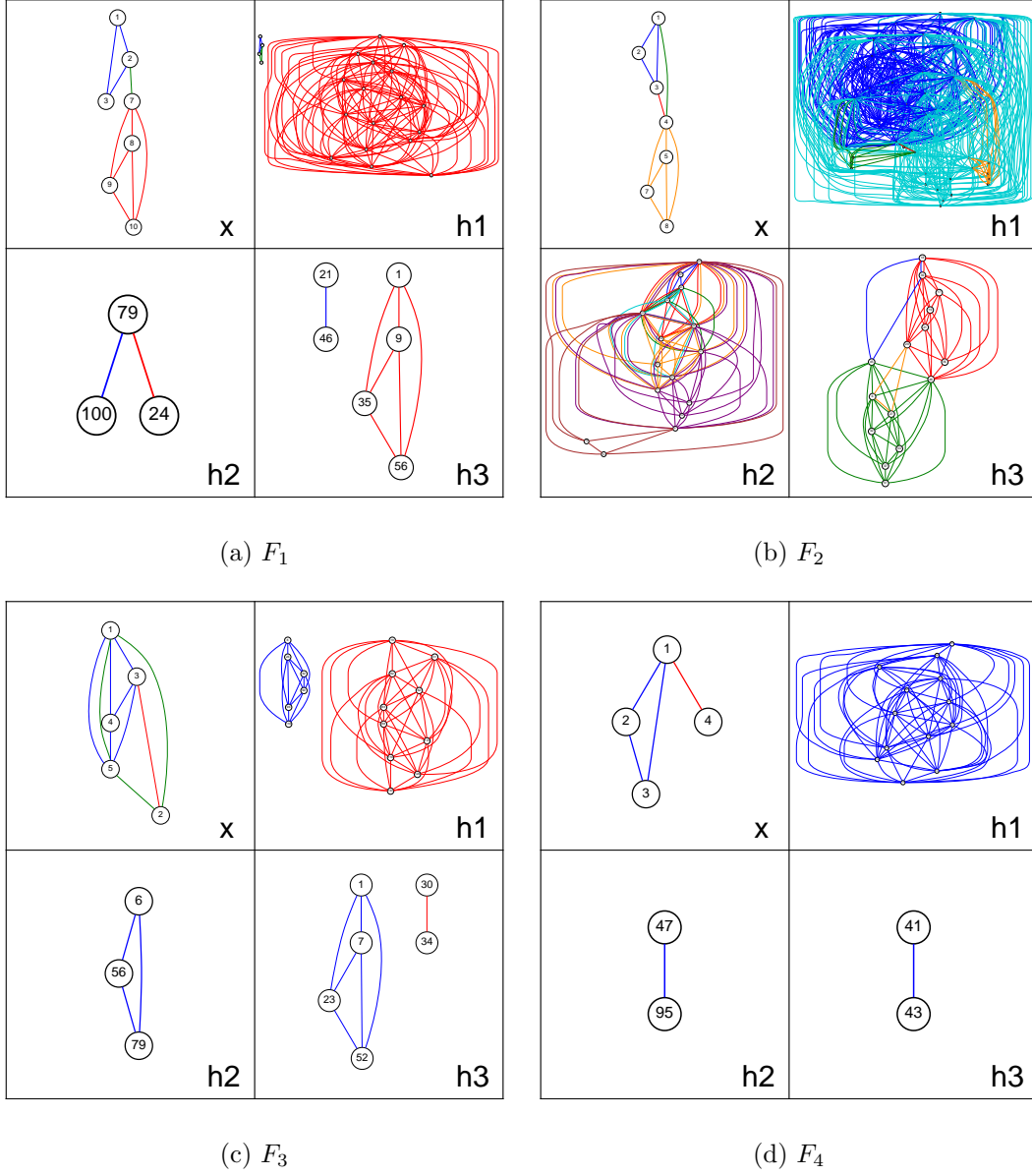


Figure 8: Same visualizations as in Figure 7 except now the interaction visualizations correspond to datasets that are all synthetic.

Table 5: Interactions detected by NID when applied to input features and the hidden layers of a neural network. Results for various datasets are shown. Under the “layer” column, “x” corresponds to input features. “h1”, “h2”, and “h3” correspond to hidden units at the first, second, and third hidden layers respectively.

datasets	layer	detected interactions
kin8nm	x	{1, 2, 3, 4, 5, 6, 7, 8}
	h1	{28, 41, 63, 75, 77, 85, 91}, {45, 54, 81, 84, 107, 136, 138, 140}, {17, 22, 23, 29, 55, 70, 127}, {22, 32, 45, 54, 70, 77, 79, 95, 127, 133, 136}, {7, 16, 17, 23, 25, 28, 41, 42, 45, 54, 75, 107, 117, 122, 127, 135}, {69, 81, 91, 127, 129}, {27, 37, 42, 43, 45, 46, 47, 54, 91, 122, 129, 131}, {16, 23, 27, 32, 39, 42, 79, 91, 99, 117, 133, 138}
	h2	{9, 49, 55}, {22, 49}, {9, 30, 55}, {11, 23, 30, 49, 57, 85, 100}
	h3	{34, 47}, {7, 27, 57}
	x	{1, 2}, {4, 5}
cal housing	h1	{18, 30, 38}, {11, 30, 38, 48, 51, 53, 72, 120}, {30, 38, 40, 48, 55, 57, 88}
	h2	{12, 34}, {2, 12, 59, 67}, {5, 59}, {20, 67, 100}
	h3	{38, 59}, {26, 40, 59}, {7, 57}
elevators	x	{2, 4, 5, 6}
	h1	{6, 13, 22, 35, 78, 79, 86, 102, 111, 120}, {48, 64, 68, 79, 98, 102, 110, 111, 112}, {6, 13, 22, 35, 37, 47, 78, 112, 114, 120}, {34, 64, 102, 114}
	h2	{14, 19, 22, 49, 55, 92}
	h3	{3, 18, 22, 31}
higgs boson	x	{1, 2}, {2, 7}, {1, 5}, {2, 3, 6, 13}, {1, 3, 4, 6}
	h1	{32, 39, 121, 123}, {2, 4, 8, 19, 29, 55, 66, 81, 95, 121, 126}, {2, 29, 84, 90}
	h2	{2, 28, 43}, {31, 42, 53}
	h3	{18, 32, 34}, {3, 11}
F_1	x	{1, 2, 3}, {7, 8, 9, 10}, {2, 7}
	h1	{10, 11, 20, 33, 36, 50, 58, 59, 61, 67, 70, 76, 77, 93, 94, 101, 133}, {65, 79, 128}, {19, 65, 128}
	h2	{79, 100}, {24, 79}
	h3	{21, 46}, {1, 9, 35, 56}
F_2	x	{1, 2, 3}, {3, 4}, {1, 4}, {4, 5, 7, 8}
	h1	{35, 54, 134}, {1, 22, 25, 32, 41, 44, 55, 57, 59, 68, 69, 72, 73, 75, 77, 80, 90, 98, 103, 104, 114, 117, 121, 127, 134, 135}, {54, 87, 90, 119, 134, 139}, {10, 21, 42, 63, 67, 73, 124}, {1, 10, 22, 36, 41, 42, 44, 54, 55, 56, 61, 72, 73, 80, 90, 102, 103, 104, 106, 121, 125, 127, 130, 134}
	h2	{27, 42, 65, 95}, {27, 44, 48, 59, 65, 95}, {44, 51, 65, 95}, {13, 27, 44, 48, 51, 59, 64, 71}, {44, 48, 64, 65, 95}, {21, 23, 27, 44, 48, 51, 64, 71, 91}, {19, 27, 44, 79, 91}
	h3	{18, 39, 45}, {17, 18, 19, 21, 29, 35, 39, 46}, {6, 27, 32, 33, 37, 45, 46, 51}, {6, 27, 29}
F_3	x	{1, 3, 4, 5}, {2, 3}, {1, 2, 5}
	h1	{8, 26, 42, 90, 96, 116}, {19, 31, 62, 82, 83, 88, 115, 119, 126, 133}
	h2	{6, 56, 79}
	h3	{1, 7, 23, 52}, {30, 34}
F_4	x	{1, 2, 3}, {1, 4}
	h1	{22, 36, 38, 42, 64, 89, 93, 97, 98, 103, 114, 119, 138}
	h2	{47, 95}
	h3	{41, 43}

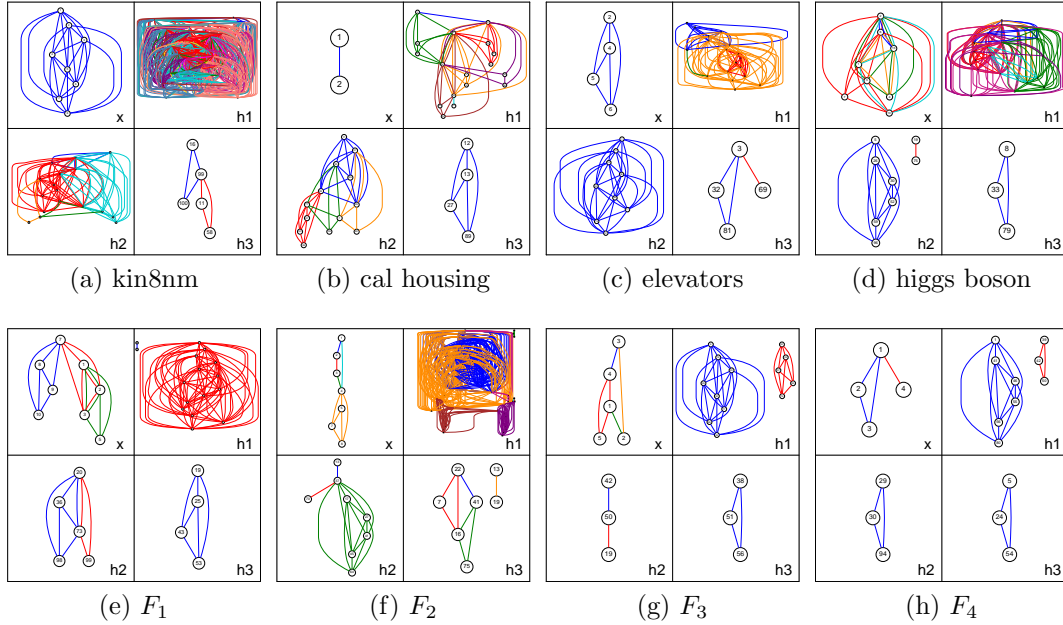


Figure 9: Same visualizations as in Figures 7 and 8 except now NID was used to interpret neural networks with 100 hidden units at every hidden layer.

6 Conclusion

In this paper, we propose a framework for interpreting the weights of a deep neural network to identify the statistical interactions it captures. Because deep neural networks can represent data well, our framework is naturally capable of accurately detecting statistical interactions in data. The framework is not only accurate, but also highly efficient at detecting interactions, by avoiding an exponential search over all possible interaction candidates of arbitrary order. Through empirical evaluation, we show that our approach is generally orders of magnitude faster than the state-of-the-art, and it achieves better detection performance on synthetic data while providing insights into both real-world data and neural network behavior. We present our framework as a new tool for interpreting a neural network and detecting statistical interactions in complex data. We plan on investigating the use of NID to detect interactions in function-generated data when features are hidden from the neural network. Moreover, since the framework requires little modification to a neural network architecture, we envision our approach applied to recurrent and convolutional neural networks, to better interpret these models as well.

Acknowledgments

We would like to thank Xinran He, Natali Ruchansky, Meisam Razaviyayn, Nancy Tsang, and anonymous reviewers for their helpful feedback and insights. This work was graciously supported by USC Annenberg Fellowships for MT and DC.

References

- Adam-Bourdarios, Claire, Cowan, Glen, Germain, Cecile, Guyon, Isabelle, Kegl, Balazs, and Rousseau, David. Learning to discover: the higgs boson machine learning challenge. URL <https://higgsml.lal.in2p3.fr/documentation/>, 2014.
- Benjamini, Yoav and Hochberg, Yosef. Controlling the false discovery rate: a practical and powerful approach to multiple testing. *Journal of the royal statistical society. Series B (Methodological)*, pp. 289–300, 1995.
- Bien, Jacob, Taylor, Jonathan, and Tibshirani, Robert. A lasso for hierarchical interactions. *Annals of statistics*, 41(3):1111, 2013.
- Bullen, PS, Mitrinović, DS, and Vasić, PM. Means and their inequalities, mathematics and its applications, 1988.
- Camachol, Rui. Inducing models of human control skills. In *European Conference on Machine Learning*, pp. 107–118. Springer, 1998.
- Caruana, Rich, Lou, Yin, Gehrke, Johannes, Koch, Paul, Sturm, Marc, and Elhadad, Noemie. Intelligible models for healthcare: Predicting pneumonia risk and hospital 30-day readmission. In *Proceedings of the 21th ACM SIGKDD International Conference on Knowledge Discovery and Data Mining*, pp. 1721–1730. ACM, 2015.
- Che, Zhengping, Purushotham, Sanjay, Khemani, Robinder, and Liu, Yan. Distilling knowledge from deep networks with applications to healthcare domain. *arXiv preprint arXiv:1512.03542*, 2015.
- Choi, Edward, Bahadori, Mohammad Taha, Sun, Jimeng, Kulas, Joshua, Schuetz, Andy, and Stewart, Walter. Retain: An interpretable predictive model for healthcare using reverse time attention mechanism. In *Advances in Neural Information Processing Systems*, pp. 3504–3512, 2016.
- Christensen, Ronald. *Plane answers to complex questions: the theory of linear models*. Springer Science & Business Media, 2011.
- Doshi-Velez, Finale and Kim, Been. A roadmap for a rigorous science of interpretability. *arXiv preprint arXiv:1702.08608*, 2017.
- Fan, Yingying, Kong, Yinfei, Li, Daoji, and Lv, Jinchu. Interaction pursuit with feature screening and selection. *arXiv preprint arXiv:1605.08933*, 2016.
- Fisher, Ronald Aylmer. *Statistical methods for research workers*. Genesis Publishing Pvt Ltd, 1925.
- Garson, G David. Interpreting neural-network connection weights. *AI Expert*, 6(4):46–51, 1991.
- Goh, ATC. Back-propagation neural networks for modeling complex systems. *Artificial Intelligence in Engineering*, 9(3):143–151, 1995.
- Goodfellow, Ian, Bengio, Yoshua, and Courville, Aaron. *Deep Learning*. MIT Press, 2016. <http://www.deeplearningbook.org>.
- Hechtlinger, Yotam. Interpretation of prediction models using the input gradient. *arXiv preprint arXiv:1611.07634*, 2016.

- Hooker, Giles. Discovering additive structure in black box functions. In *Proceedings of the tenth ACM SIGKDD international conference on Knowledge discovery and data mining*, pp. 575–580. ACM, 2004.
- Itti, Laurent, Koch, Christof, and Niebur, Ernst. A model of saliency-based visual attention for rapid scene analysis. *IEEE Transactions on pattern analysis and machine intelligence*, 20(11):1254–1259, 1998.
- Jakobs, K. and Seez, C. The higgs boson discovery. *Scholarpedia*, 10(9):32413, 2016. revision 151683.
- Kim, Been. *Interactive and interpretable machine learning models for human machine collaboration*. PhD thesis, Massachusetts Institute of Technology, 2015.
- Kim, Been, Koyejo, Oluwasanmi O, and Khanna, Rajiv. Examples are not enough, learn to criticize! criticism for interpretability. In *Advances In Neural Information Processing Systems*, pp. 2280–2288, 2016.
- Krause, Josua, Perer, Adam, and Ng, Kenney. Interacting with predictions: Visual inspection of black-box machine learning models. In *Proceedings of the 2016 CHI Conference on Human Factors in Computing Systems*, pp. 5686–5697. ACM, 2016.
- LeCun, Yann, Bengio, Yoshua, and Hinton, Geoffrey. Deep learning. *Nature*, 521(7553):436–444, 2015.
- Lipton, Zachary C. The mythos of model interpretability. *arXiv preprint arXiv:1606.03490*, 2016.
- Loh, Wei-Yin. Regression tress with unbiased variable selection and interaction detection. *Statistica Sinica*, pp. 361–386, 2002.
- Lou, Yin, Caruana, Rich, Gehrke, Johannes, and Hooker, Giles. Accurate intelligible models with pairwise interactions. In *Proceedings of the 19th ACM SIGKDD international conference on Knowledge discovery and data mining*, pp. 623–631. ACM, 2013.
- Maaten, Laurens van der and Hinton, Geoffrey. Visualizing data using t-sne. *Journal of Machine Learning Research*, 9(Nov):2579–2605, 2008.
- Mahendran, Aravindh and Vedaldi, Andrea. Understanding deep image representations by inverting them. In *Proceedings of the IEEE Conference on Computer Vision and Pattern Recognition*, pp. 5188–5196, 2015.
- Mnih, Volodymyr, Heess, Nicolas, Graves, Alex, et al. Recurrent models of visual attention. In *Advances in neural information processing systems*, pp. 2204–2212, 2014.
- Mnih, Volodymyr, Kavukcuoglu, Koray, Silver, David, Rusu, Andrei A, Veness, Joel, Bellemare, Marc G, Graves, Alex, Riedmiller, Martin, Fidjeland, Andreas K, Ostrovski, Georg, et al. Human-level control through deep reinforcement learning. *Nature*, 518(7540):529–533, 2015.
- Murray, Richard M, Li, Zexiang, Sastry, S Shankar, and Sastry, S Shankara. *A mathematical introduction to robotic manipulation*. CRC press, 1994.
- Needell, Deanna, Ward, Rachel, and Srebro, Nati. Stochastic gradient descent, weighted sampling, and the randomized kaczmarz algorithm. In *Advances in Neural Information Processing Systems*, pp. 1017–1025, 2014.

- Pace, R Kelley and Barry, Ronald. Sparse spatial autoregressions. *Statistics & Probability Letters*, 33(3):291–297, 1997.
- Provost, Foster J, Fawcett, Tom, et al. Analysis and visualization of classifier performance: Comparison under imprecise class and cost distributions. In *KDD*, volume 97, pp. 43–48, 1997.
- Rasmussen, CE, Neal, RM, Hinton, G, Van Camp, D, Revow, M, Ghahramani, Z, Kustra, R, and Tibshirani, R. Delve. university of toronto, 2003.
- Rendle, Steffen. Factorization machines. In *Data Mining (ICDM), 2010 IEEE 10th International Conference on*, pp. 995–1000. IEEE, 2010.
- Ribeiro, Marco Tulio, Singh, Sameer, and Guestrin, Carlos. Why should i trust you?: Explaining the predictions of any classifier. In *Proceedings of the 22nd ACM SIGKDD International Conference on Knowledge Discovery and Data Mining*, pp. 1135–1144. ACM, 2016.
- Simonyan, Karen, Vedaldi, Andrea, and Zisserman, Andrew. Deep inside convolutional networks: Visualising image classification models and saliency maps. *arXiv preprint arXiv:1312.6034*, 2013.
- Sorokina, Daria. *Modeling Additive Structure and Detecting Interactions with Groves of Trees*. PhD thesis, Cornell University, 2008a.
- Sorokina, Daria, Caruana, Rich, Riedewald, Mirek, and Fink, Daniel. Detecting statistical interactions with additive groves of trees. In *Proceedings of the 25th international conference on Machine learning*, pp. 1000–1007. ACM, 2008b.
- Székel, Gábor J, Rizzo, Maria L, Bakirov, Nail K, et al. Measuring and testing dependence by correlation of distances. *The Annals of Statistics*, 35(6):2769–2794, 2007.
- Varshney, Kush R and Alemzadeh, Homa. On the safety of machine learning: Cyber-physical systems, decision sciences, and data products. *arXiv preprint arXiv:1610.01256*, 2016.
- Wonnacott, Thomas H and Wonnacott, Ronald J. *Introductory statistics*, volume 19690. Wiley New York, 1972.
- Wood, Simon. *Generalized additive models: an introduction with R*. CRC press, 2006.
- Xu, Kelvin, Ba, Jimmy, Kiros, Ryan, Cho, Kyunghyun, Courville, Aaron C, Salakhutdinov, Ruslan, Zemel, Richard S, and Bengio, Yoshua. Show, attend and tell: Neural image caption generation with visual attention. In *ICML*, volume 14, pp. 77–81, 2015.
- Yosinski, Jason, Clune, Jeff, Nguyen, Anh, Fuchs, Thomas, and Lipson, Hod. Understanding neural networks through deep visualization. *arXiv preprint arXiv:1506.06579*, 2015.